A new nonlinear real-time filter based on Free Energy

JUAN ANDRÉS ROTETA LANNES[1], ANDRES GABRIEL GARCIA[2],
OSVALDO ENRIQUE AGAMENNONI[3]

[1]Universidad Tecnológica Nacional - Comisión de Investigaciones Científicas,
Facultad Regional Bahía Blanca, Grupo de Investigación en Multifísica Aplicada,
11 de abril 461, Bahía Blanca,Buenos Aires,
ARGENTINA

[2]Universidad Tecnológica Nacional, Facultad Regional Bahía Blanca,
Grupo de Estudio Sobre Energía - Departamento de Ingenieria Electrica,
11 de abril 461, Bahía Blanca, Buenos Aires,
ARGENTINA

[3]CONICET - Universidad Nacional del Sur,
Instituto de Investigaciones en Ingeniería Eléctrica “Alfredo Desages”,
San Andrés 800, Bahía Blanca, Buenos Aires,
ARGENTINA

Abstract: - This study introduces a novel non-linear real-time filter based on the concept of Free Energy, which is applied to estimate the state of mobile robots in dynamic environments. By leveraging the principles of Bayesian inference, the proposed Free Energy Filter aims to minimize prediction errors between the observed and estimated trajectories. The approach extends existing non-linear filtering techniques, incorporating elements such as the Fokker-Planck equation. The simulation results demonstrate the effectiveness of this method in improving the control accuracy of unicycle robots equipped with the Bessel controller. The study also discusses comparisons with traditional Kalman filtering, highlighting the advantages of the proposed approach in adapting to noisy and uncertain conditions.

Key-Words: - Free-Energy, Fokker-Planck, Stochastic, Kalman Filter

Received: April 9, 2025. Revised: May 18, 2025. Accepted: July 19, 2025. Published: November 14, 2025.

1 Introduction

The concept of ”Free Energy” is central to the theory that views the brain as a system striving to minimize uncertainty or surprise in its perceptions and actions. This idea, widely developed by [1], [2], [3], [4], and his colleagues, [5], [6], is rooted in Bayesian inference principles. It provides a unifying framework to explain how the brain processes sensory information, makes predictions, and learns from its environment.

Essentially, the brain is modeled as a system that constantly makes inferences about the state of the world based on noisy and partial sensory data. To reduce the uncertainty of these inferences, the brain updates its internal models of the world by minimizing a quantity known as ”Free Energy.” This minimization is equivalent to adjusting the predictions generated by the brain so that they are more consistent with the observed sensory signals, achieved through continuous feedback between expectations (predictions) and the perceived reality (sensory data).

In the context of a mobile robot, the Free Energy framework can be applied to develop control algorithms that allow the robot to navigate and adapt to a dynamic environment. Here, the algorithm would aim to minimize the discrepancy between predicted and observed trajectories, continuously adjusting its movements and decisions to maintain a state of low free energy, in other words, a state in which the robot’s actions are more aligned with its internal model predictions about the environment.

This approach provides a robust and adaptable method for controlling autonomous systems, allowing the robot not only to react to changes in the environment but also to anticipate and proactively adjust its behavior to maintain optimal performance.

The structure of this study unfolds as follows. We begin with the introduction of the necessary definitions and notation, followed by the presentation of the unicycle robot with the Bessel controller and closed-form trajectory solutions in Section 2.

The subsequent sections delve into the Free-Energy concept and Kalman Filter in sections 2.2 and sections 2.3 respectively.

In Section 3, we present the Free-Energy Filter. Section 3.1 provides an introduction to the Free Energy Principle, while Section 3.2 outlines the problem statement. In Section 3.3, we discuss a specific case involving the Unicycle Robot equipped with the Bessel Controller. This section includes an analysis based on two Taylor expansion approaches: the integration first-order Taylor expansion, discussed in Section 3.3.1, and the second-order Taylor expansion, detailed in Section 3.3.2.

Section 4 is devoted to Simulation, where we provide practical examples and simulation results. In Section 6, we present the results obtained from the simulations.

The conclusion offers insights and outlines avenues for future research in Section 7. We discuss potential future Research in Section 7.1.

2 Notation and Definitions: Preliminaries

In this section, some definitions are provided for the sake of completeness.

2.1 Unicycle Robot with Bessel's Controller

In this study, unicycle robots are considered (Figure 1 and Eq. 1):

$$\begin{bmatrix} \dot{x}_1 \\ \dot{x}_2 \\ \dot{x}_3 \end{bmatrix} = \begin{bmatrix} \cos\Theta & 0 \\ \sin\Theta & 0 \\ 0 & 1 \end{bmatrix} \begin{bmatrix} U_1 \\ U_2 \end{bmatrix} \tag{1}$$

where, the control inputs $(U_1, U_2) \in \Re^1 \times \Re^1$

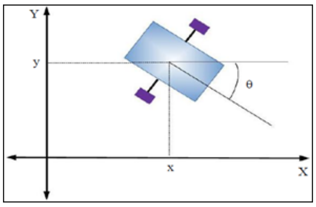

Figure 1: Unicycle-like robot with coordinates. *Source: created by the authors*

According to [7], asymptotic stability can be achieved for this kind of robot globally using the following controller Eq. 2

$$\begin{cases} U_1 = a3C_1J_1(\Theta)\Theta^2 + 5aC_2J_2(\Theta)\Theta^3 \\ U_2 = a\Theta \end{cases} \tag{2}$$

With Bessel of the first order:

$$\begin{cases} J_1(\Theta) = \frac{\Theta}{2} - \frac{\Theta^3}{48} + \frac{\Theta^5}{384} + O^6 \\ J_2(\Theta)\frac{\Theta^2}{8} - \frac{\Theta^4}{96} + O^6 \end{cases}$$

Resulting in the control according to [7], as follows (Eq. 3)

$$\begin{cases} U_1 = a3C_1(\frac{\Theta}{2} - \frac{\Theta^3}{48} + \frac{\Theta^5}{384})\Theta^2 + 5aC_2(\frac{\Theta^2}{8} - \frac{\Theta^4}{96})\Theta^3 \\ U_2 = a\Theta \end{cases} \tag{3}$$

2.2 Free-Energy concept

The following equation is a key component in the extended formulation of the "Free-Energy" model, which seeks to implement in a biologically plausible way how perceptual systems can differentially weigh sources of sensory information based on their noise level. This equation helps to understand how the neural network can learn to recognize features encoded in covariance patterns among sensory inputs and how these representations can be adjusted through experience and continuous learning.

$$\min_{p(y,\tilde{y})} \int q(\tilde{y}) Ln \frac{p(y,\tilde{y})}{q(\tilde{y})} d\tilde{y} \tag{4}$$

Given $q(\tilde{y})$ as a probability density function (PDF), for example, a Dirac delta distribution. Here, y represents the real perception or measurement and $\tilde{y}$ represents the estimate given by the algorithm of the system.

Specifically, it describes an update to the model's variables that allows capturing the uncertainty associated with the different features of the stimuli.

2.3 Kalman Filter

The Kalman filter is maybe the most famous algorithm in the area of estimation and control, and it is still the reference point when someone wants to compare a new filter, even if the assumptions of Kalman are not always valid. The filter works in two steps, one step is the prediction where the state is propagated using the system model, and the second step is the correction where the prediction is adjusted with the real measurement. By doing this alternation between prediction and correction the error goes down and the estimation becomes better.

The Kalman filter is optimal only in linear systems with Gaussian noise, and this is something that everybody repeats, but it is still true, so when the system is non-linear or when the noise is not Gaussian the Kalman filter does not perform so well. Nevertheless, because it is simple and fast it has been used for decades in many engineering applications, from control of vehicles to robotics and signal processing, [8], [9].

In this work we are using Kalman filter not as the main tool but more as a reference. We compare our Free Energy filter with it, so the reader can see what is better and what is worse. The comparison is made in the particular case of the unicycle robot with the Bessel controller, so both filters are applied under the same conditions. In this way it is more fair to evaluate if the new method really brings an improvement or not.

3 Free-Energy Filter

3.1 Free Energy Principle

The Free Energy principle was originally developed by Karl Friston and it has been applied a lot in neuroscience, but here we try to use the same logic for a robotic system. The principle says that a system, if it wants to keep stability and adapt to changes, must reduce the difference between what it expects and what it really perceives. This difference is usually called prediction error or Free Energy, and the minimization of it is the central mechanism.

In other words, the system has an internal model of the world and then it receives new data from sensors. If the data and the model are not aligned, then the system feels surprise, so it changes the model or it changes its actions, and little by little the surprise gets smaller. This is why the principle is powerful, because it explains perception and action in one single framework.

For robots, the same principle can be very useful. Robots are always working in environments with noise and uncertainty, and they need to act in real time. By minimizing Free Energy, the robot can adapt better and keep the estimation of states closer to the reality. It is not only reacting but also anticipating, which is something very important when the conditions are changing quickly.

Mathematically, the principle can be expressed in Eq. 5, which is the same form that we already introduced before in Eq. 4:

$$\min_{p(y,\tilde{y})} \int q(\tilde{y}) Ln \frac{p\,(y,\tilde{y})}{q(\tilde{y})} d\tilde{y} \quad (5)$$

This equation shows that the system is trying to make the approximate posterior $q(\tilde{y})$ closer to the real joint distribution $p(y,\tilde{y})$. The meaning is simple: the closer they are, the less surprise, the less Free Energy.

The terms of the equation can be explained like this:

1. $q(\tilde{y})$ is the approximate distribution of the hidden variables, it is basically what the system believes after observing.
2. The fraction inside the logarithm compares what is predicted with what is real, so if there is a big difference the Free Energy is large, and if they are similar then the Free Energy is small.

So the general idea is not complicated, although the equations look hard at first sight. The principle gives a way to adjust continuously the states of the system so that prediction and observation are aligned as much as possible.

3.2 Problem Statement

Let us consider a nonlinear system with noise described as follows:

$$\begin{cases} \dot{x}(t) = f(x,\mu) + \hat{\mu}\,\xi_1 \\ y(t) = C\tilde{x}(t) + \xi_y \end{cases}$$

Where:

- The first equation represents the real system,
- The third represents the real measurement.

Furthermore, ξ_n is defined as a general source noise.

The Free Energy Minimization Problem is then formulated as [5]:

$$\min_{x} Ln\, p(x(t),\tilde{x}(t),\hat{\mu}) \quad (6)$$

Applying the Fokker-Planck equation to the system, [10], we get:

$$\frac{\partial p}{\partial t} = -\sum_{i=1}^{n} \frac{\partial}{\partial x_i}(f_i(x(t),\mu)\cdot p(x(t),\hat{x}(t))) + \sum_{i=1}^{n}\sum_{j=1}^{m} \frac{\partial^2}{\partial x_i \partial x_j}(\frac{1}{2}\hat{\mu}\hat{\mu}^T p(x(t),\tilde{x}(t)))$$

We now introduce a variable separation for the joint probability.

$$p(x(t),\tilde{x}(t)) = p(x,\tilde{x},\mu)\cdot\varphi(t)$$

Thus, the updated Fokker-Planck equation becomes:

$$p(x,\tilde{x},\mu)\cdot\dot{\varphi}(t) = -\sum_{i=1}^{n} \frac{\partial}{\partial x_i}(f_i(x,\mu)\cdot p(x,\tilde{x}(t))\cdot\varphi(t)) + \sum_{i=1}^{n}\sum_{j=1}^{m} \frac{\partial^2}{\partial x_i \partial x_j}(\frac{1}{2}\hat{\mu}\hat{\mu}^T p(x,\tilde{x}\cdot\varphi(t))$$

This can be further simplified to the following.

$$p(x,\tilde{x},\mu)\cdot\dot{\varphi}(t) = -\left(\sum_{i=1}^{n}\frac{\partial}{\partial x_i}(f_i(x,\mu)\cdot p(x,\tilde{x})\right)\cdot\varphi(t) + \left(\sum_{i=1}^{n}\sum_{j=1}^{m}\frac{\partial^2}{\partial x_i\partial x_j}\left(\frac{1}{2}\hat{\mu}^T\hat{\mu}p(x,\tilde{x}\right)\right)\cdot\varphi(t)$$

We then redefine two key terms for clarity.

$$\Psi(x,\hat{x},\mu) = \sum_{i=1}^{n}\frac{\partial}{\partial x_i}(f_i(x,\mu)\cdot p(x,\tilde{x})$$

$$\Phi(x,\tilde{x},\hat{\mu}) = \sum_{i=1}^{n}\sum_{j=1}^{m}\frac{\partial^2}{\partial x_i\partial x_j}(\frac{1}{2}\hat{\mu}^T\hat{\mu}p(x,\tilde{x})$$

Thus, the ratio of the scaled probability becomes:

$$\frac{p(x,\tilde{x},\mu)}{-\Psi(x,\hat{x},\mu)+\Phi(x,\tilde{x},\hat{\mu})} = \frac{\varphi(t)}{\dot{\varphi}(t)} = \frac{1}{\alpha}$$

We return to the Free Energy minimization problem (Eq. 6), where:

$$\alpha = \frac{-\Psi(x,\hat{x},\mu)+\Phi(x,\tilde{x},\hat{\mu})}{p(x,\tilde{x},\mu)}$$

We now redefine two terms for simplification.

$$\beta_1(x,\hat{x},\mu) = \frac{-\Psi(x,\hat{x},\mu)}{p(x,\tilde{x},\mu)}$$

$$\beta_2(x,\hat{x},\mu) = \frac{\sum_{i=1}^{n}\sum_{j=1}^{m}\frac{\partial^2}{\partial x_i\partial x_j}(p(x,\tilde{x})}{p(x,\tilde{x},\mu)}$$

Thus:

$$\alpha = \beta_1(x,\hat{x},\mu)+\beta_2(x,\hat{x},\mu)\frac{1}{2}\hat{\mu}^2 \tag{7}$$

Finally, recalling the Free Energy minimization condition (Eq.6) and defining $\alpha = 0$ (in Eq.7), we arrive at the final equation.

$$\begin{cases} \min\limits_{x} Ln\ p(x,\tilde{x},\hat{\mu}) \\ 0 = \sum_{i=1}^{n}\frac{\partial}{\partial x_i}(f_i(x,\mu)\cdot p(x,\tilde{x}) \\ +\sum_{i=1}^{n}\sum_{j=1}^{m}\frac{\partial^2}{\partial x_i\partial x_j}(p(x,\tilde{x})\frac{1}{2}\hat{\mu}^2 \\ = \beta_1(x,\hat{x},\mu)+\beta_2(x,\hat{x},\mu)\frac{1}{2}\hat{\mu}^2 \end{cases} \tag{8}$$

3.3 Particular case: Unicycle Robot with Bessel Controller

Taking as a particular case the model of the unicycle robot along with the control presented in the paper *"Asymptotic Stability of Unicycle-Like Robots: The Bessel's Controller"* by Garcia 2020, as previously mentioned, the following set of state equations is derived.

$$\begin{cases} f_1 = \dot{x}_1 = \cos\Theta(3aC_1\frac{\Theta^3}{2} - aC_1\frac{\Theta^5}{16} + 3aC_1\frac{\Theta^7}{384} \\ + 5aC_2\frac{\Theta^5}{8} - 5aC_2\frac{\Theta^7}{96}) \\ f_2 = \dot{x}_2 = \sin\Theta(3aC_1\frac{\Theta^3}{2} - aC_1\frac{\Theta^5}{16} + 3aC_1\frac{\Theta^7}{384} \\ + 5aC_2\frac{\Theta^5}{8} - 5aC_2\frac{\Theta^7}{96}) \\ f_3 = \dot{x}_3 = a\Theta \end{cases}$$

In this case, the variables x_1 and x_2 are not present in f_1, f_2 and f_3, so:

$$\begin{cases} \frac{df_1}{d\Theta} = -\sin\Theta \\ \left(3aC_1\frac{\Theta^3}{2} - aC_1\frac{\Theta^5}{16} + 3aC_1\frac{\Theta^7}{384} + 5aC_2\frac{\Theta^5}{8} - 5aC_2\frac{\Theta^7}{96}\right) \\ +\cos\Theta \\ \left(9aC_1\frac{\Theta^2}{2} - 5aC_1\frac{\Theta^4}{16} + 21aC_1\frac{\Theta^6}{384} + 25aC_2\frac{\Theta^4}{8} - 35aC_2\frac{\Theta^6}{96}\right) \\ \\ \frac{df_2}{d\Theta} = \cos\Theta \\ \left(3aC_1\frac{\Theta^3}{2} - aC_1\frac{\Theta^5}{16} + 3aC_1\frac{\Theta^7}{384} + 5aC_2\frac{\Theta^5}{8} - 5aC_2\frac{\Theta^7}{96}\right) \\ +\sin\Theta \\ \left(9aC_1\frac{\Theta^2}{2} - 5aC_1\frac{\Theta^4}{16} + 21aC_1\frac{\Theta^6}{384} + 25aC_2\frac{\Theta^4}{8} - 35aC_2\frac{\Theta^6}{96}\right) \\ \\ \frac{df_3}{d\Theta} = a \end{cases}$$

Next, we substitute the approximate Taylor series for $\cos(\Theta)$ and $\sin(\Theta)$:

$$\begin{cases} \cos(\theta) \approx 1 - \frac{1}{2}\theta^2 + \frac{1}{24}\theta^4 - \frac{1}{720}\theta^6 \\ \sin(\theta) \approx 1 - \frac{1}{2}\theta^2 + \frac{1}{24}\theta^4 - \frac{1}{720}\theta^6 \end{cases}$$

This results in the following.

$$\begin{cases} f_1 = \dot{x}_1 = \left(1 - \frac{1}{2}\Theta^2 + \frac{1}{24}\Theta^4 - \frac{1}{720}\Theta^6\right) \\ \left(3aC_1\frac{\Theta^3}{2} - aC_1\frac{\Theta^5}{16} + 3aC_1\frac{\Theta^7}{384} + 5aC_2\frac{\Theta^5}{8} - 5aC_2\frac{\Theta^7}{96}\right) \\ \\ f_2 = \dot{x}_2 = \left(\Theta - \frac{\Theta^3}{6} + \frac{\Theta^5}{120} - \frac{\Theta^7}{5040}\right) \\ \left(3aC_1\frac{\Theta^3}{2} - aC_1\frac{\Theta^5}{16} + 3aC_1\frac{\Theta^7}{384} + 5aC_2\frac{\Theta^5}{8} - 5aC_2\frac{\Theta^7}{96}\right) \\ f_3 = y = a\Theta \end{cases}$$

The distribution of terms is as follows.

$$\begin{cases} f_1 = \dot{x}_1 = \\ \left(3aC_1\frac{\Theta^3}{2} - aC_1\frac{\Theta^5}{16} + 3aC_1\frac{\Theta^7}{384} + 5aC_2\frac{\Theta^5}{8} - 5aC_2\frac{\Theta^7}{96}\right) \\ -\frac{1}{2}\Theta^2 \\ \left(3aC_1\frac{\Theta^3}{2} - aC_1\frac{\Theta^5}{16} + 3aC_1\frac{\Theta^7}{384} + 5aC_2\frac{\Theta^5}{8} - 5aC_2\frac{\Theta^7}{96}\right) \\ +\frac{1}{24}\Theta^4 \\ \left(3aC_1\frac{\Theta^3}{2} - aC_1\frac{\Theta^5}{16} + 3aC_1\frac{\Theta^7}{384} + 5aC_2\frac{\Theta^5}{8} - 5aC_2\frac{\Theta^7}{96}\right) \\ -\frac{1}{720}\Theta^6 \\ \left(3aC_1\frac{\Theta^3}{2} - aC_1\frac{\Theta^5}{16} + 3aC_1\frac{\Theta^7}{384} + 5aC_2\frac{\Theta^5}{8} - 5aC_2\frac{\Theta^7}{96}\right) \\ \\ f_2 = \dot{x}_2 = \\ \Theta\left(3aC_1\frac{\Theta^3}{2} - aC_1\frac{\Theta^5}{16} + 3aC_1\frac{\Theta^7}{384} + 5aC_2\frac{\Theta^5}{8} - 5aC_2\frac{\Theta^7}{96}\right) \\ -\frac{\Theta^3}{6} \\ \left(3aC_1\frac{\Theta^3}{2} - aC_1\frac{\Theta^5}{16} + 3aC_1\frac{\Theta^7}{384} + 5aC_2\frac{\Theta^5}{8} - 5aC_2\frac{\Theta^7}{96}\right) \\ +\frac{\Theta^5}{120} \\ \left(3aC_1\frac{\Theta^3}{2} - aC_1\frac{\Theta^5}{16} + 3aC_1\frac{\Theta^7}{384} + 5aC_2\frac{\Theta^5}{8} - 5aC_2\frac{\Theta^7}{96}\right) \\ -\frac{\Theta^7}{5040} \\ \left(3aC_1\frac{\Theta^3}{2} - aC_1\frac{\Theta^5}{16} + 3aC_1\frac{\Theta^7}{384} + 5aC_2\frac{\Theta^5}{8} - 5aC_2\frac{\Theta^7}{96}\right) \\ \\ f_3 = y = a\Theta \end{cases}$$

Taking partial derivatives.

$$\begin{cases} \frac{df_1}{d\Theta} = \left(-1 + \frac{1}{2}\Theta^2 - \frac{1}{24}\Theta^4 + \frac{1}{720}\Theta^6\right) \\ \left(3aC_1\frac{\Theta^3}{2} - aC_1\frac{\Theta^5}{16} + 3aC_1\frac{\Theta^7}{384} + 5aC_2\frac{\Theta^5}{8} - 5aC_2\frac{\Theta^7}{96}\right) \\ +\left(1 - \frac{1}{2}\Theta^2 + \frac{1}{24}\Theta^4 - \frac{1}{720}\Theta^6\right) \\ \left(9aC_1\frac{\Theta^2}{2} - 5aC_1\frac{\Theta^4}{16} + 21aC_1\frac{\Theta^6}{384} + 25aC_2\frac{\Theta^4}{8} - 35aC_2\frac{\Theta^6}{96}\right) \\ \\ \frac{df_2}{d\Theta} = \left(1 - \frac{1}{2}\Theta^2 + \frac{1}{24}\Theta^4 - \frac{1}{720}\Theta^6\right) \\ \left(3aC_1\frac{\Theta^3}{2} - aC_1\frac{\Theta^5}{16} + 3aC_1\frac{\Theta^7}{384} + 5aC_2\frac{\Theta^5}{8} - 5aC_2\frac{\Theta^7}{96}\right) \\ +\left(1 - \frac{1}{2}\Theta^2 + \frac{1}{24}\Theta^4 - \frac{1}{720}\Theta^6\right) \\ \left(9aC_1\frac{\Theta^2}{2} - 5aC_1\frac{\Theta^4}{16} + 21aC_1\frac{\Theta^6}{384} + 25aC_2\frac{\Theta^4}{8} - 35aC_2\frac{\Theta^6}{96}\right) \\ \\ \frac{df_3}{d\Theta} = a \end{cases}$$

Returning to Equation 8, for the proposed model, it becomes:

$$0 = -\left(\frac{\partial f_1(\Theta)}{\partial\Theta} + \frac{\partial f_2(\Theta)}{\partial\Theta} + \frac{\partial f_3(\Theta)}{\partial\Theta}\right)$$
$$P(\Theta, \hat{\Theta}, \hat{\mu}) - (f_1(\Theta) + f_2(\Theta) + f_3(\Theta))$$
$$\frac{\partial P(\Theta, \hat{\Theta}, \hat{\mu})}{\partial\Theta} + \frac{\partial^2 P(\Theta, \hat{\Theta}, \hat{\mu})}{\partial\Theta^2}\frac{1}{2}\hat{\mu}^2$$

We rewrite to simplify: $F_1(\Theta) = \frac{\partial f_1(\Theta)}{\partial\Theta} + \frac{\partial f_2(\Theta)}{\partial\Theta} + \frac{\partial f_3(\Theta)}{\partial\Theta}$ and $F_2(\Theta) = f_1(\Theta) + f_2(\Theta) + f_3(\Theta)$, resulting in:

$$\frac{1}{2}\hat{\mu}^2\frac{\partial^2 P(\Theta, \hat{\Theta}, \hat{\mu})}{\partial\Theta^2} =$$
$$F_1(\Theta)P(\Theta, \hat{\Theta}, \hat{\mu}) - F_2(\Theta)\frac{\partial P(\Theta, \hat{\Theta}, \hat{\mu})}{\partial\Theta}$$

To minimize $\min_{\Theta} \ln\ p^*(\Theta, \hat{\Theta}, \hat{\mu})$, we assume that theta is near Θ^* and with $F_2(\Theta^*)\frac{\partial P}{\partial\Theta} \approx 0$:

$$\frac{1}{2}\hat{\mu}^2\frac{\partial^2 P(\Theta^*, \hat{\Theta}, \mu)}{\partial\Theta^2} = F_1(\Theta^*)P(\Theta, \hat{\Theta}, \hat{\mu})$$

This leads to the following.

$$\frac{\partial^2}{\partial\Theta^2}\ln P(\Theta, \hat{\Theta}, \mu) \approx$$
$$\frac{1}{P(\Theta, \hat{\Theta}, \mu)}\frac{\partial P(\Theta, \hat{\Theta}, \mu)}{\partial\Theta}$$

Thus:

$$\frac{\partial^2}{\partial\Theta^2}\ln P(\Theta, \hat{\Theta}, \mu) \approx \frac{2}{\hat{\mu}^2}F_1(\Theta) \tag{9}$$

For $\Theta \to \Theta^*$.

At this point, solutions are sought through two different ways:

3.3.1 Taylor expansion of order 1 around θ^* and subsequent integration

If we expand $\ln P(\Theta, \hat{\Theta}, \mu)$ around $\Theta \rightarrow \Theta^*$and integrate (Eq. 9), we get the following.

$$(\frac{\partial}{\partial\Theta}\ln P(\Theta^*, \hat{\Theta}, \mu)) - (\frac{\partial}{\partial\Theta}\ln P(\hat{\Theta}, \hat{\Theta}, \mu)) \approx \frac{2}{\hat{\mu}^2}\int_{\hat{\Theta}}^{\Theta^*} F_1(\Theta)\cdot d\Theta$$

$$\ln P(\Theta, \hat{\Theta}, \mu) = \ln P(\Theta^*, \hat{\Theta}, \mu) + \left(\frac{\partial \ln P(\Theta, \hat{\Theta}, \mu)}{\partial\Theta}\Big|_{\Theta=\Theta^*}\right)(\Theta - \Theta^*) + O(2)$$

Differentiating:

$$\frac{\partial}{\partial\Theta}\ln P(\Theta, \hat{\Theta}, \mu) \approx \frac{\partial \ln P(\Theta, \hat{\Theta}, \mu)}{\partial\Theta}\Big|_{\Theta=\Theta^*} = constant$$

Evaluating between Θ and Θ^*, we get the following.

$$0 = \int_{\hat{\Theta}}^{\Theta^*} F_1(\Theta)\cdot d\Theta = G(\Theta^*) - G(\hat{\Theta})$$

The resulting expression is as follows:

$$\begin{aligned} 0 = G(\Theta^*) - G(\hat{\Theta}) = &-\frac{a\,(3\,C_1 - 20\,C_2)\left(\Theta^{*15} - \hat{\Theta}^{15}\right)}{29030400} - \frac{a\,(3\,C_1 - 20\,C_2)\left(\Theta^{*14} - \hat{\Theta}^{14}\right)}{3870720} \\ &+ \frac{a\,(5\,C_1 - 36\,C_2)\left(\Theta^{*13} - \hat{\Theta}^{13}\right)}{838656} + \frac{a\,(19\,C_1 - 140\,C_2)\left(\Theta^{*12} - \hat{\Theta}^{12}\right)}{552960} \\ &- \frac{a\,(171\,C_1 - 1120\,C_2)\left(\Theta^{*11} - \hat{\Theta}^{11}\right)}{887040} - \frac{a\,(33\,C_1 - 200\,C_2)\left(\Theta^{*10} - \hat{\Theta}^{10}\right)}{38400} \\ &+ \frac{a\,(59\,C_1 - 300\,C_2)\left(\Theta^{*9} - \hat{\Theta}^{9}\right)}{17280} + \frac{a\,(39\,C_1 - 140\,C_2)\left(\Theta^{*8} - \hat{\Theta}^{8}\right)}{3072} \\ &- \frac{5\,a\,(C_1 - 2\,C_2)\left(\Theta^{*7} - \hat{\Theta}^{7}\right)}{112} - \frac{a\,(13\,C_1 - 10\,C_2)\left(\Theta^{*6} - \hat{\Theta}^{6}\right)}{96} \\ &+ \frac{3\,C_1\,a\left(\Theta^{*5} - \hat{\Theta}^{5}\right)}{10} + \frac{3\,C_1\,a\left(\Theta^{*4} - \hat{\Theta}^{4}\right)}{8} + \frac{a\left(\Theta^{*2} - \hat{\Theta}^{2}\right)}{2} \end{aligned}$$

3.3.2 Taylor expansion of order 2 around θ^*

As an alternative to the previous point, if the first term of the Eq. 9 is assumed to be zero; then:

$$0 = \frac{2}{\hat{\mu}^2}F_1(\Theta^*) - \frac{2}{\hat{\mu}^2}F_1(\hat{\Theta})$$

equivalent to

$$0 = F_1(\Theta^*) - F_1(\hat{\Theta})$$

The resulting expression is as follows:

$$
\begin{aligned}
0 = {} & a\Theta^* \cdot \frac{8709120\,C_1}{967680} + a(\Theta^*)^2 \cdot \frac{17418240\,C_1}{967680} \\
& -a(\Theta^*)^3 \cdot \frac{15724800\,C_1}{967680} - a(\Theta^*)^4 \cdot \frac{9072000\,C_1}{967680} \\
& +a(\Theta^*)^3 \cdot \frac{12096000\,C_2}{967680} + a(\Theta^*)^5 \cdot \frac{4127760\,C_1}{967680} \\
& +a(\Theta^*)^4 \cdot \frac{18144000\,C_2}{967680} + a(\Theta^*)^6 \cdot \frac{1665216\,C_1}{967680} \\
& -a(\Theta^*)^5 \cdot \frac{14817600\,C_2}{967680} - a(\Theta^*)^7 \cdot \frac{598752\,C_1}{967680} \\
& -a(\Theta^*)^6 \cdot \frac{8467200\,C_2}{967680} - a(\Theta^*)^8 \cdot \frac{184680\,C_1}{967680} \\
& +a(\Theta^*)^7 \cdot \frac{3628800\,C_2}{967680} + a(\Theta^*)^9 \cdot \frac{43890\,C_1}{967680} \\
& +a(\Theta^*)^8 \cdot \frac{1209600\,C_2}{967680} + a(\Theta^*)^{10} \cdot \frac{9900\,C_1}{967680} \\
& -a(\Theta^*)^9 \cdot \frac{323400\,C_2}{967680} - a(\Theta^*)^{11} \cdot \frac{1638\,C_1}{967680} \\
& -a(\Theta^*)^{10} \cdot \frac{71280\,C_2}{967680} - a(\Theta^*)^{12} \cdot \frac{273\,C_1}{967680} \\
& +a(\Theta^*)^{11} \cdot \frac{10920\,C_2}{967680} + a(\Theta^*)^{12} \cdot \frac{1820\,C_2}{967680} \\
& -a\hat{\Theta} \cdot \frac{8709120\,C_1}{967680} - a(\hat{\Theta})^2 \cdot \frac{17418240\,C_1}{967680} \\
& +a(\hat{\Theta})^3 \cdot \frac{15724800\,C_1}{967680} + a(\hat{\Theta})^4 \cdot \frac{9072000\,C_1}{967680} \\
& -a(\hat{\Theta})^3 \cdot \frac{12096000\,C_2}{967680} - a(\hat{\Theta})^5 \cdot \frac{4127760\,C_1}{967680} \\
& -a(\hat{\Theta})^4 \cdot \frac{18144000\,C_2}{967680} - a(\hat{\Theta})^6 \cdot \frac{1665216\,C_1}{967680} \\
& +a(\hat{\Theta})^5 \cdot \frac{14817600\,C_2}{967680} + a(\hat{\Theta})^7 \cdot \frac{598752\,C_1}{967680} \\
& +a(\hat{\Theta})^6 \cdot \frac{8467200\,C_2}{967680} + a(\hat{\Theta})^8 \cdot \frac{184680\,C_1}{967680} \\
& -a(\hat{\Theta})^7 \cdot \frac{3628800\,C_2}{967680} - a(\hat{\Theta})^9 \cdot \frac{43890\,C_1}{967680} \\
& -a(\hat{\Theta})^8 \cdot \frac{1209600\,C_2}{967680} - a(\hat{\Theta})^{10} \cdot \frac{9900\,C_1}{967680} \\
& +a(\hat{\Theta})^9 \cdot \frac{323400\,C_2}{967680} + a(\hat{\Theta})^{11} \cdot \frac{1638\,C_1}{967680} \\
& +a(\hat{\Theta})^{10} \cdot \frac{71280\,C_2}{967680} + a(\hat{\Theta})^{12} \cdot \frac{273\,C_1}{967680} \\
& -a(\hat{\Theta})^{11} \cdot \frac{10920\,C_2}{967680} - a(\hat{\Theta})^{12} \cdot \frac{1820\,C_2}{967680}
\end{aligned}
$$

4 Simulation

In this section we explain how we did the simulations that are used to test the Free Energy filter and to compare it with the Kalman filter. The simulations were made in MATLAB with Simulink, because this platform is very common and also allows us to represent the system with blocks that are easy to connect. In this way we can build a model of the robot and the filters and then see how they behave when noise is added.

The general structure of the simulation is shown in Figure 2(Appendix). We created four main blocks. The first one is the Robot Dynamics block, where we simulate the kinematic equations of the unicycle robot together with the control inputs of the Bessel controller. This block gives the trajectory of the robot in a way that is close to what would happen in real life.

The second block is the Control block, which applies the Bessel controller and generates the actions. This is important because the Bessel controller is what makes the robot stable and it is also what defines the type of trajectory that will be followed.

The third block is the Kalman Filter block. Here we implemented the classical Kalman filter, so that we can have a reference to compare. Even if we know that Kalman filter has limitations, it is still the baseline in filtering problems.

Finally, the fourth block is the Free Energy Filter block. This block contains the equations that we derived before and it updates the estimated state by minimizing Free Energy. The idea is that this block should adapt better to noise and nonlinearities compared with the Kalman filter.

The interaction between the blocks produces a complete simulation where we can see the robot trajectory, the estimation of the states, and also the errors of both filters. The outputs of the simulation include graphs of trajectories and graphs of estimation error, so it is easy to see the difference between the two methods.

We also tested with different noise conditions. In the first case we used a noise power of 0.01 with a sample time of 0.1, which is a relatively low noise situation. In the second case we used a noise power of 0.5 with a sample time of 0.01, which is stronger noise and more difficult for the filters. This way we can evaluate how robust each filter is in different scenarios.

The important point of this section is not only to show that the Free Energy filter works, but also to show that it works under the same conditions where the Kalman filter is tested, so the comparison is fair and the conclusions are reliable.

5 Materials and Methods

All simulations were performed on a Core M1 Apple laptop with 4GB RAM, using MATLAB release 2023b. The ODE113 (Adams) solver was employed with a maximum relative tolerance error of 1e-1.

6 Results and Discussion

In this section we look at the results that came out of the simulations and we try to understand what they mean for the Free Energy filter compared with the Kalman filter. The focus is on the estimation of the state of the unicycle robot when the Bessel controller is used, because this was the main test case.

Figure 3 (Appendix) and Figure 5 (Appendix) show the estimated angles in both filters, while Figure 4 (Appendix) and Figure 6 (Appendix) show the errors. By looking at these plots it is possible to see some clear tendencies.

From the results it can be seen that when the noise is small both filters work reasonably well, but the Free Energy filter of second order gives smoother estimates. When the noise is bigger the difference is more clear, because the Kalman filter starts to show bigger errors and the Free Energy filter still adapts better. This indicates that the Free Energy filter is more robust when the conditions are not ideal.

It is also interesting that the first order Free Energy filter, when it is applied, sometimes performs worse than Kalman. This is a limitation of the first order approximation, because it is too simple to capture the nonlinearities. On the other hand, the second order expansion gives results that are clearly better in both cases of noise, which shows that the order of the approximation is an important factor.

Another point is that the computational cost of the Free Energy filter is similar to the Kalman filter. This is important because if the filter was too slow then it would not be useful for real-time control, but here we see that it can be applied in real time without problems.

So, in summary, the discussion shows that the Free Energy filter of second order is a better option than Kalman when there is uncertainty and strong noise. The first order version is not always better, but it still provides some insight, and the second order version is the one that really makes the difference.

7 Conclusion

This study introduced a Free Energy-based nonlinear filter as an advanced solution for real-time control and state estimation in mobile robotics. The simulations demonstrated that, while the first-order FE filter may not consistently outperform the Kalman filter, the second-order FE filter delivers superior results under both tested noise conditions. Its ability to handle nonlinear dynamics and adapt to non-Gaussian noise establishes its robustness and practical utility.

The computational efficiency of the FE filter and the straightforward implementation make it a promising candidate for integration into low-power embedded systems. These characteristics suggest its potential for broad application across diverse robotic platforms and scenarios.

Future work will focus on refining the FE filter for higher efficiency, extending its application to more complex systems, and conducting comparative studies with other filtering methods. These advancements could further establish the FE filter as a leading solution for real-time robotic navigation and control.

7.1 Future Research

- Conduct a comparative analysis with other advanced filtering techniques.
- Extending the application of the FE filter to larger and more complex robotic systems.
- Developing generalized versions of the FE filter for broader applications.

References:

[1] Karl Friston, A theory of cortical responses, *Philosophical Transactions of the Royal Society B: Biological Sciences*, Volume 360, 2005, Pages 815-816, https://doi.org/10.1098/rstb.2005.1622.

[2] Karl Friston, The free-energy principle: A unified brain theory?, *Nature Reviews Neuroscience*, Volume 11, 2010, Pages 127-138, ISSN 1471-003X, https://doi.org/10.1038/nrn2787.

[3] Karl Friston and James Kilner and Lee Harrison, A free energy principle for the brain, *Journal of Physiology Paris*, Volume 100, 2006, Pages 70-87, ISSN 0928-4257, https://doi.org/10.1016/j.jphysparis.2006.10.001.

[4] Karl Friston, A free energy principle for biological systems, *Entropy*, Volume 14, 2012, Pages 2100-2121, ISSN 1099-4300, https://doi.org/10.3390/e14112100.

[5] Rafal Bogacz, A tutorial on the free-energy framework for modeling perception and learning, *Journal of Mathematical Psychology*, Volume 76, Part B, 2017, Pages 198-211, ISSN 0022-2496, https://doi.org/10.1016/j.jmp.2015.11.003.

[6] Christopher L Buckley and Chang Sub Kim and Simon McGregor and Anil K Seth, The free energy principle for action and perception: A mathematical review, *Journal of Mathematical Psychology*, Volume 81, 2017, Pages 55-79, ISSN 0022-2496, https://doi.org/10.1016/j.jmp.2017.09.004.

[7] García, Andrés Gabriel, Asymptotic Stability of Unicycle-Like Robots: The Bessel's Controller, *Journal of Mechatronics and Robotics*, Volume 4, 2020, Pages 1-7, https://doi.org/10.3844/jmrsp.2020.1.7.

[8] Huibert Kwakernaak and Raphael Sivan, Linear Optimal Control Systems, , 1972.

[9] Nicholas Assimakis, Maria Adam, ”I/O SNR and Noise Covariances Norm Ratio Relation in Kalman Filter,” WSEAS Transactions on Systems and Control, vol. 19, pp. 373-378, 2024, https://doi.org/10.37394/23203.2024.19.40.

[10] Y. Sun and M. Kumar, Nonlinear Bayesian filtering based on Fokker-Planck equation and tensor decomposition, *18th International Conference on Information Fusion (Fusion), Washington, DC, USA*, 2015, Pages 1483-1488, https://ieeexplore.ieee.org/document/7266732.

Contribution of Individual Authors to the Creation of a Scientific Article (Ghostwriting Policy)

The authors equally contributed in the present research, at all stages from the formulation of the problem to the final findings and solution.

Sources of Funding for Research Presented in a Scientific Article or Scientific Article Itself

No funding was received for conducting this study.

Conflict of Interest

The authors have no conflicts of interest to declare that are relevant to the content of this article.

APPENDIX

This appendix includes the additional figures related to the simulations presented in this work. It shows the complete Simulink model used for testing the Free Energy Filter, together with the comparative results that illustrate the estimation behavior and error performance under different noise conditions.

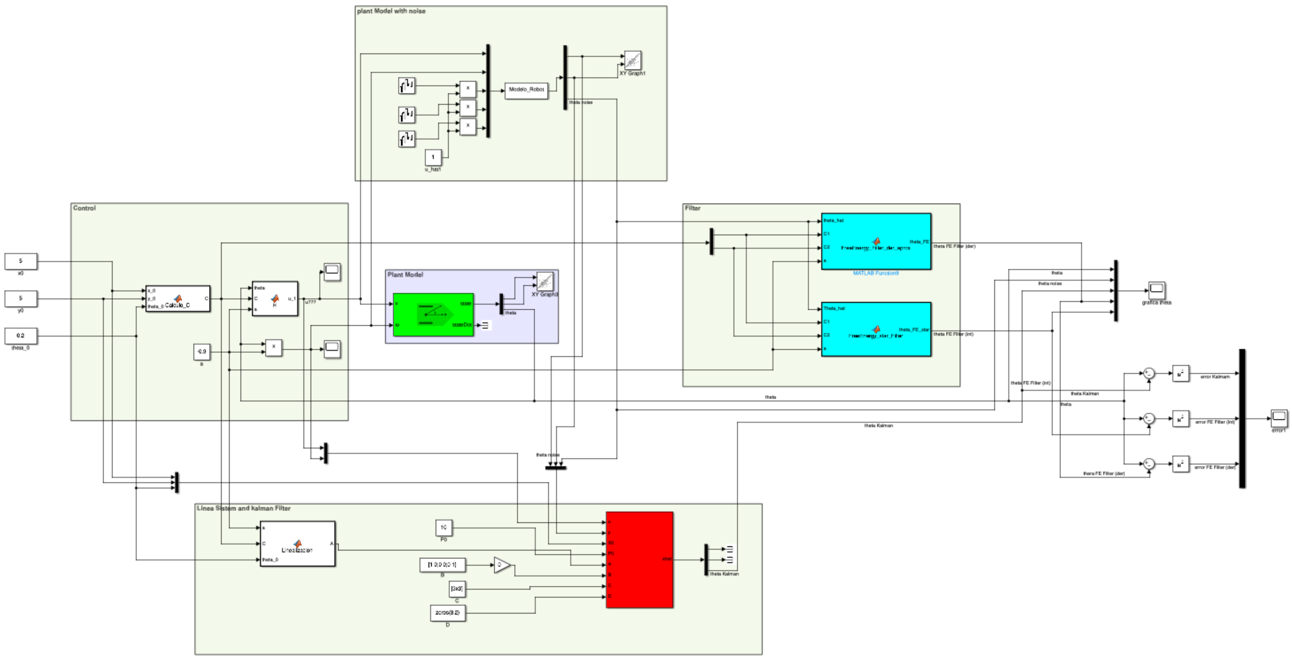

Figure 2: Simulink Model. *Source: created by the authors*

Figure 3: Comparative angle graph with noise type 1. *Source: created by the authors*

Juan Andrés Roteta Lannes,
Andres Gabriel Garcia, Osvaldo Enrique Agamennoni

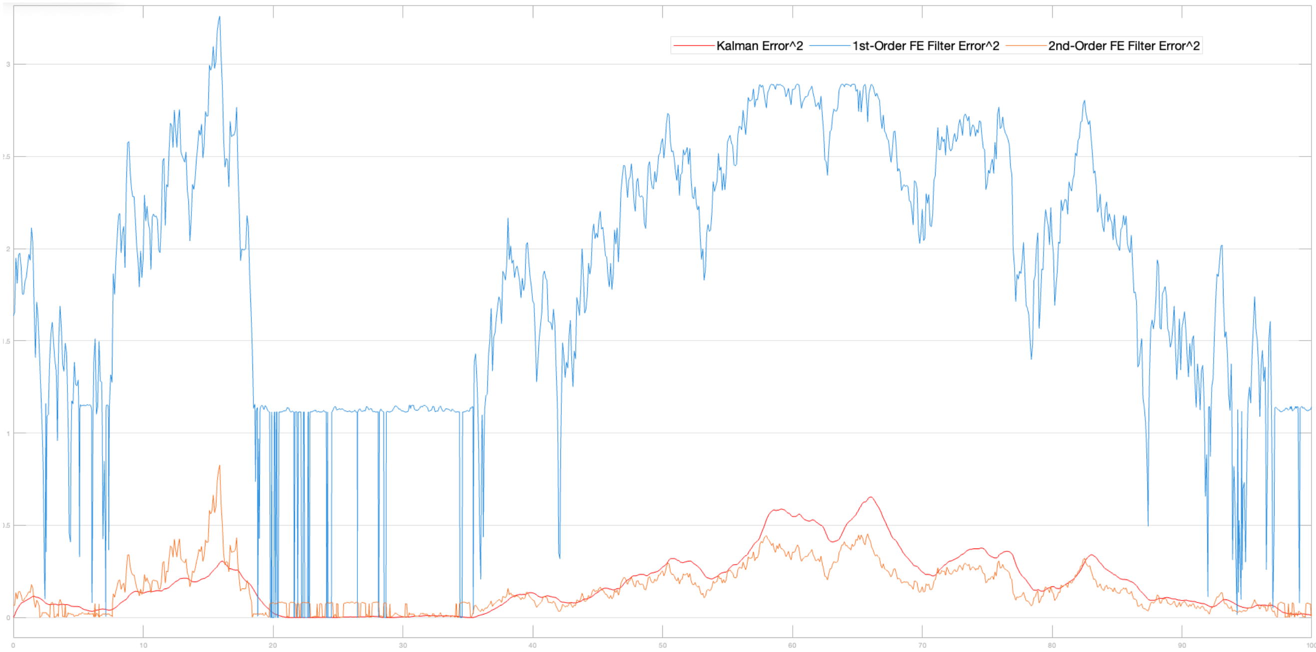

Figure 4: Comparative error with noise type 1. *Source: created by the authors*

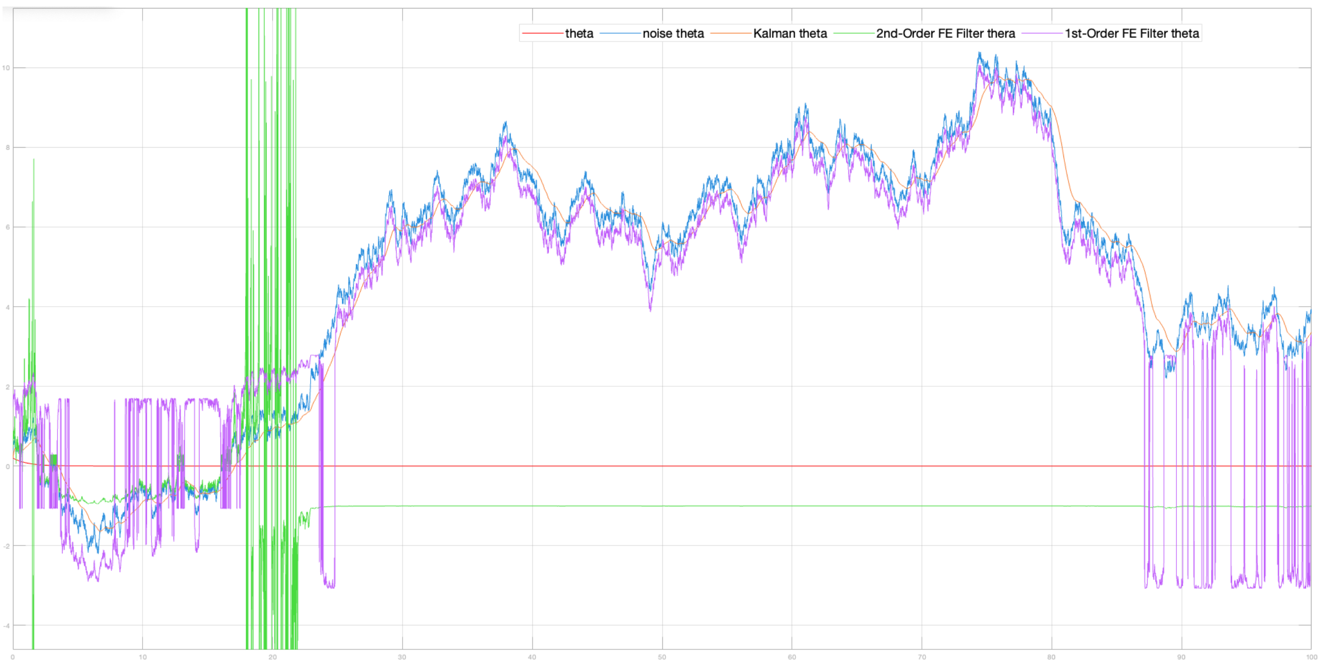

Figure 5: Comparative angle graph with noise type 2. *Source: created by the authors*

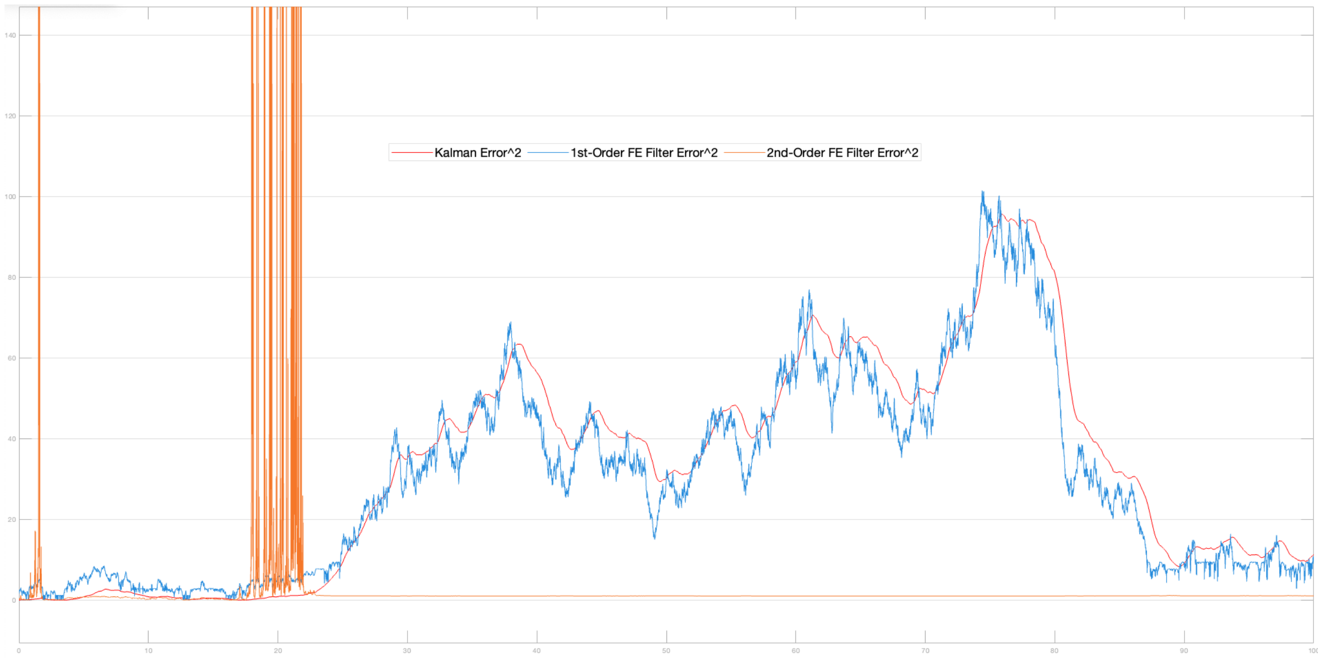

Figure 6: Comparative error with noise type 2. *Source: created by the authors*